Silicon-based Hybrid Integrated Photonic Chip for K_u band Electromagnetic Wave Sensing

Chi-Jui Chung*, Xiaochuan Xu*, *Member, IEEE*, Zeyu Pan, *Student Member, IEEE*, Farzad Mokhtari-Koushyar, Rui Wang, Hai Yan, Harish Subbaraman, *Member, IEEE*, Ray T. Chen, *Fellow, OSA & IEEE*

***Abstract*—In this paper, we experimentally demonstrate a highly sensitive on-chip photonic electromagnetic wave sensor operating at 14.1 GHz with a 3 dB bandwidth of 4.84 GHz. The demonstrated electromagnetic sensor has several important advantages over conventional electrical electromagnetic sensors including high sensitivity, compact in size and strong immunity to electromagnetic interference (EMI). The sensor is comprised of a bowtie antenna and an asymmetric Mach-Zehnder interferometer (MZI). One arm of the MZI is an electro-optic (EO) polymer infiltrated one-dimensional (1D) slot photonic crystal waveguide (SPCW) and the other is a strip waveguide with teeth of subwavelength pitch. Bowtie antennas are designed and optimized to effectively collect 14.1 GHz microwave signal and applies it across the SPCW. The phase of the light guided in the SPCW therefore changes, and so does the amplitude of the output end of the MZI. The sensor is only 4.6 mm × 4.8 mm in size and has a low insertion loss of ~ 10 dB. Experimental results show the limit of detection at 14.1 GHz is 4.31 mW/m^2, which is corresponding to a minimum detectable electric field of 1.8 V/m**

***Index Terms*—Slow light, microwave photonics, photonic crystal, optical polymer, microwave receiver, integrated optics.**

I. Introduction

On-chip photonic electromagnetic (EM) wave sensors have been attracting considerable attention in recent years [1-4]. This photonic sensing approach detects microwave signals via photons and thus eliminates the need of discrete electronics components for high-speed signal transmission, amplification, and power conditioning, which are commonly used in conventional electrical microwave sensors [5, 6]. Therefore, photonic EM wave sensors have eminent advantages over the traditional electrical counterparts in terms of immunity to electromagnetic interference (EMI), high speed operation, power consumption, and footprint [4, 7]. These advantages make high sensitivity and accurate on-chip EM sensors a promising approach for high performance wireless communication [2, 8, 9]and sensing applications [1, 3, 10].

One crucial element in a high performance on-chip photonic EM wave sensor is an efficient electro-optic(EO) phase shifter, in which the enhanced electrical field provided by antennas modulates the refractive index of the active material with EO effect and subsequently changes the phase of light guided in the phase shifter. Various phase shifter designs have been proposed such as plasmonic/EO polymer hybrid structure [4], EO polymer waveguides [1, 2], lithium niobate waveguides [8], and silicon/EO polymer hybrid structure [11, 12]. Among these structures, plasmonic/EO polymer hybrid structure shows smallest footprint and is intrinsically capable of operating at high frequency due to the small resistance. However, the high propagation loss (>1 dB/μm) of plasmonic waveguide [13] and the high insertion loss of the mode converter limit the performance due to the trade-off between interaction length and optical loss. Moreover, the stringent fabrication alignment (<50 nm) between metal and waveguide makes it difficult to implement. The pure EO polymer and lithium niobate waveguides are not compatible with standard complementary metal-oxide-semiconductor (CMOS) fabrication process. In addition, both materials have lower refractive indices compared to silicon, resulting in large footprint. EO polymer infiltrated silicon slot waveguides, which combine the advantages of the high refractive index of silicon and large EO effect in EO polymer, have also been studied intensively [14, 15]. When equipped with slow light structures, the effective in-device r_{33} in slow light slot waveguide can be greatly enhanced, making it a promising candidate for high performance EM wave sensors.

Slow light two-dimensional (2D) photonic crystal silicon/polymer hybrid phase shift structure has high optical propagation loss [16] and is frail to fabrication errors [17]. One-dimensional (1D) slot photonic crystal waveguide (SPCW) has been reported with lower optical propagation loss when compared with 2D SPCWs, due to less etched surface area overlapped with optical mode while maintaining similar slow light effect [18]. Among EO polymer infiltrated 1D SPCW, 2D SPCW and conventional slotted waveguide, 1D SPCW has the best figure-of-merit $f = \sigma \cdot n_g \cdot L_{3dB}$ [19] where σ is the ratio of

This work was supported by Air Force Office of Scientific Research (AFOSR) Multidisciplinary University Research Initiative (MURI) Center on Silicon Nanomembrane (Contract No. FA9550-08-1-0394), the Air Force Research Lab (AFRL) Small Business Technology Transfer Research (STTR) program (Contract No. FA8650-14-C-5015), and Omega Optics Inc.

C.J. Chung, Z. Pan, F. Mokhtari-Koushyar, R. Wang, H. Yan, and R. T. Chen are with the Microelectronic Research Center, Department of Electrical and Computer Engineering, University of Texas, Austin, TX 78758 USA (e-mail: cjchung@utexas.edu; panzeyu@utexas.edu; mokhtari@utexas.edu; ruiwang.utaustin@utexas.edu; hai.yan@utexas.edu; chen@ece.utexas.edu).

X. Xu is with Omega Optics, Inc., Austin, TX 78757, USA (e-mail: xiaochuan.xu@omegaoptics.com).

H. Subbaraman is with Department of Electrical and Computer Engineering, Boise State University, Boise, Idaho 83725, USA (e-mail: harishsubbaraman@boisestate.edu)

*The authors contribute to the paper equally.

Color versions of one or more of the figures in this paper are available online at http://ieeexplore.ieee.org.

Digital Object Identifier

This article has been accepted for publication in a future issue of this journal, but has not been fully edited. Content may change prior to final publication. Citation information: DOI 10.1109/JLT.2017.2784382, Journal of Lightwave Technology

optical mode in the EO polymer region, n_g is the group index, and L_{3dB} is the length of the phase shifter in millimeters with 3 dB propagation loss. Therefore, EO polymer infiltrated 1D SPCW has the potential to perform better than 2D SPCW and slotted waveguide as an EO phase shifter.

In this paper, we design and demonstrate a compact and highly sensitive on-chip photonic EM waver sensor operating at 14.1 GHz with 3 dB bandwidth of 4.84 GHz. 14.1 GHz falls into K_u band and can be applied to satellite communications for both civilian and military networks [20]. The proposed sensor features a set of bowtie antenna and a Mach-Zehnder interferometer (MZI) structure with one arm of slow-light enhanced EO polymer infiltrated 1D SPCW and the other arm of silicon strip waveguide with teeth of subwavelength pitch, as shown in Figure 1(a). The device region is doped with two-step ion implantation. The doping profile is tailored so that the resistance at the implanted region is greatly reduced and Ohmic contact is formed. Therefore, signal voltage drop is mostly across the slot while the absorption loss is still low. A bowtie antenna is designed to harvest and concentrate electrical field of the EM wave and applies it onto the slow light enhanced EO polymer infiltrated SPCW to modulate the phase of the guided optical wave. Inverse taper couplers with polymer overlay are adopted to efficiently couple light in and out from the sensor. The proposed sensor structure takes advantages of low loss and strong slow light effect of the 1D SPCW, high electric field enhancement of the bowtie antenna, and large EO coefficient of the EO polymer, which enable the detection of an EM wave with electric field intensity of 1.8 V/m. Compared to 2.5 V/m minimum detectable electric field at 8.4 GHz reported in EO polymer infiltrated 2D SPCW paper [3], this work shows improvement due to the lower propagation loss of 1D SPCW structure while maintaining similar slow light effect. The device is only 4.6 mm × 4.8 mm in size with active region of 300 μm offering a compact solution for a vast range of EM wave applications.

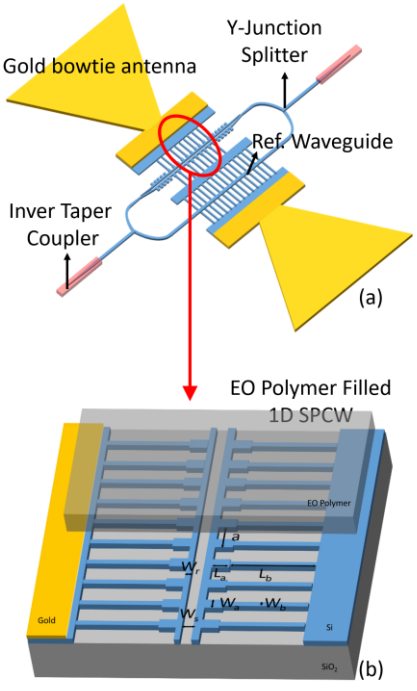

Fig. 1. (a) Schematic of the proposed sensor based on bowtie antenna coupled MZI structure. Light coupled from inverse taper coupler is spitted into two arms: one is EO polymer infiltrated 1D SPCW, and the other is strip waveguide with teeth. The phase is modulated at the arm of 1D SPCW arm and subsequently causes the output optical intensity variation when the light of the two arms interfere. (b) Schematic plot of the slow light enhanced EO polymer infiltrated 1D SPCW, which consists of a slot and two sections of teeth connected to bulk silicon.

II. Device Design

A. EO polymer infiltrated 1D SPCW phase shifter

The active arm of the MZI is the slow light enhanced EO polymer infiltrated SPCW where light slows down and is modulated by interacting with EO polymer based on the enhanced Pockels effect. The 1D SPCW is comprised of center EO polymer slot, and two sections of the silicon teeth as shown in Figure 1(b). Compared to previous reported design[19], a set of narrow teeth is used to connect the 1D SPCW to the bulk silicon region so that the voltage drop of the modulation signal mostly occurs in the slot region. The narrow teeth have subwavelength width and thus do not affect the propagation of the optical modes. The 1D SPCW is designed and optimized for 220 nm silicon-on-insulator (SOI) wafer with 3 μm buried oxide layer. An EO polymer, SEO125 (n=1.63), from Soluxra, LLC, which shows large bulk EO coefficient r_{33} of 135 pm/V, low optical loss, and good temporal stability is chosen to refill the silicon slot PCW as the top cladding layer [11]. This 1D SPCW is optimized using plane wave expansion targeting at large group index, optical confinement in slot, and slow light wavelength in vicinity of 1550 nm. The optimized period (a), tooth width a (W_a), tooth width b (W_b), tooth length a (L_a), tooth length b (L_b), slot width (W_a), and rail width (W_r) are 370 nm, 148 nm, 74 nm, 250 nm, 1750 nm, 100, and 150 nm, respectively. The 1D SPCW length is 300 μm. The photonic band diagram and the group index simulation results are shown in Figure 2, which indicates that the group index can achieve 38.05 at 1564.8 nm and the optical confinement in the EO polymer slot σ is 0.24.

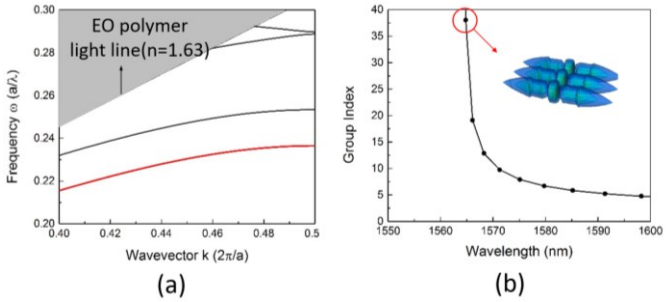

Fig. 2. (a) Photonic band diagram and (b) Group index versus wavelength of 1D SPCW using plane wave expansion method, inset is the optical modal profile.

To reduce the strong reflection at high group index interface of the 1D SPCW, we design a step taper between the 1D SPCW and regular slot waveguide using three dimensional (3D) finite difference time domain (FDTD) simulation. The coupling efficiency increases from 37% to 62% at 1554 nm as shown in Figure 3. The step taper has five periods with pitch a =350 nm, tooth width (W_t) =140 nm, tooth length (L_t) = 250 nm, and rail width (W_r) = 200 nm.

This article has been accepted for publication in a future issue of this journal, but has not been fully edited. Content may change prior to final publication. Citation information: DOI 10.1109/JLT.2017.2784382, Journal of Lightwave Technology

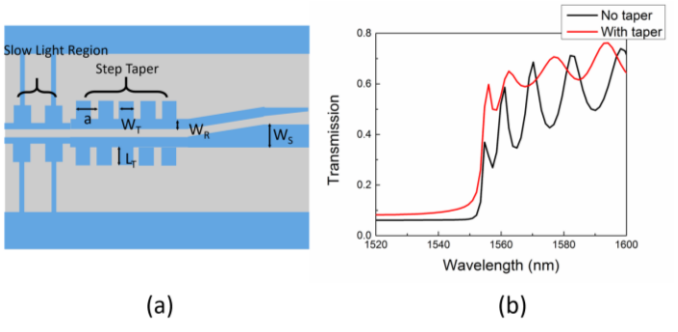

Fig. 3. (a) Schematic of the step taper section connecting silicon strip waveguide to regular slot waveguide (b) Simulated transmission spectra with (show in red) and without the step taper (show in black).

The other arm of the MZI is a strip waveguide with teeth designed also for electrical connection purpose. The structure is optimized using plane wave expansion and 3D FDTD. The optimized period, center silicon strip width, tooth width, and tooth length are 400 nm, 79.2 nm, and 1175 nm, respectively. The waveguide length is also chosen to be 300 μm. The simulated group index is 3.79 at 1550 nm. The inverse taper coupler design has been reported in previous paper [21] where the silicon waveguide width is adiabatically tapered from 450 nm (device end) to 160 nm (fiber end). A 3 μm x 3 μm SU-8 polymer waveguide is overlaid on the silicon waveguide to match the modal area of input lensed fibers. The measured averaged coupling loss per inverse taper can achieve as low as 0.62 dB.

B. Bowtie antenna and ion implantation design for 14.1GHz operation

A gold bowtie antenna with a pair of extension bars attached to the bowtie vertexes are designed to make full use of the entire length of EO interaction range [22, 23] . This antenna provides uniform electrical field enhancement in the feed gap along the extension bar direction and therefore is suitable for integrating the MZI structure in the gap. To assure the majority of the enhanced RF electrical field falls across the EO polymer infiltrated slot, two steps ion implantation are adopted to reduce RC time delay induced by bulk silicon and silicon teeth.

The schematic of the designed bowtie antenna and the implantation distribution is shown in Figure 4(a) and (b). The antenna stands on the buried oxide layer and has a thickness of 4μm, arm length of 2.3 mm, flare angle of 60 degree and extension bars of 8.4 μm × 300 μm. The gap between the extension bars is 8.4 μm. This antenna is designed to operate at 14.1 GHz. The center 7.35 μm of the MZI structure is designed to be implanted to 1×10^{17} cm^{-3} so that the increased optical loss induced by free carrier absorption isn't significant, as shown in Figure 4(b) [24]. While the two bulk silicon regions adjacent to the center region are designed to be implanted to 1×10^{20} cm^{-3} to provide low enough resistance and ensure the Ohmic contact between the gold antenna and implanted silicon. Figure 4(c) and (d) show the electric field distribution simulation results between the antenna bars at 14.1 GHz with consideration of effective radio frequency(RF) dielectric constant and effective resistivity of silicon and EO polymer are calculated based on filling factor [25, 26]. The enhanced 14.1 GHz alternative voltage (AC) electric field are accumulated at the EO polymer slot region of the 1D SPCW and has 47.72% voltage drop in the EO polymer slot region calculated by integrating the electric field in the slot divided by voltage applied on the antenna. The voltage drop percentage dedicates the resistance of the teeth and bulk silicon is low enough and the device performance won't be limited by RC delay at 14.1 GHz.

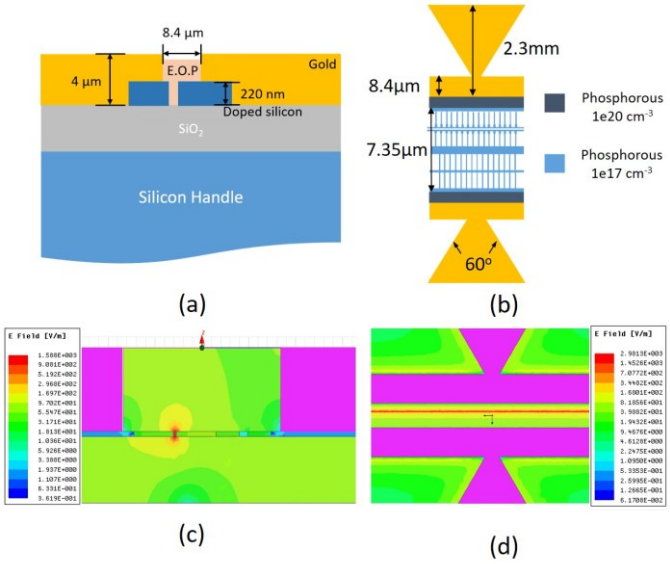

Fig. 4. (a) Side view and (b) Top view of the bowtie antenna with extension bars and ion implantation distribution (c) Side view and (d) Top view of simulated electric field distribution over the antenna gap region feeding with 14.1GHz.

III. DEVICE FABRICATION

The fabrication flow of the EM wave sensor is shown in Figure 5. The fabrication starts with an SOI chip with 220 nm device layer and 3 μm-thick buried oxide layer implanted with phosphorus of 1×10^{17} cm^{-3}. The cross-shaped platinum alignment marks are patterned for e-beam lithography alignment as illustrated in Figure 5(a). The sample is then implanted on designed opening regions with phosphorus to 1×10^{20} cm^{-3} and rapid thermal annealed at 1000 ° C for 10 seconds [see Figure 5(b)]. Next, the MZI structure, Y-junction splitter & combiner, and silicon taper for inverse taper couplers are patterned by Jeol 6000 FSE e-beam lithography system and etched by reactive ion etching (RIE) [see Figure 5(c)]. The silicon device layer in the antenna region is then etched away through photolithography and RIE so that the antenna can sit on the buried oxide layer to reduce the EM wave reflection [see Figure 5(d)]. The 3.8 μm thick antenna is electroplated using 5 nm/100 nm chromium/gold seed layer with the MZI structure region protected to avoid the contamination in the slot and teeth region. After the seed layer removal with gold and chromium etchant [see Figure 5(e)], the SU-8 inverse taper overlaid layer is patterned [see Figure 5(f)]. Finally, EO polymer is formulated, coated, and cured at 80°C in vacuum oven for overnight. Scanning electron microscope (SEM) images of the sensor are shown in Figure 6, which indicate good fabrication accuracy and fine alignment between each fabrication steps. The EO polymer is poled to align the chromophores and initiate the EO effect before waveguide cleaving and the following testing. The

poling process is conducted at the EO polymer glass transition temperature of 150°C, with an external electric field of 120 V/μm. The sensor is then cleaved at the inverse taper coupler region for light coupling.

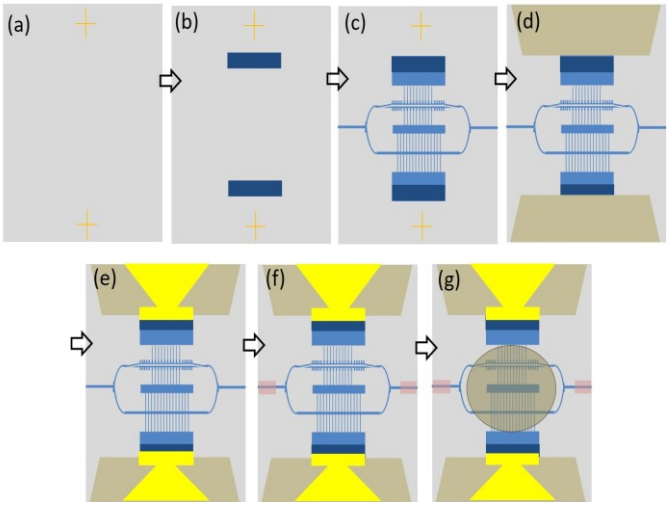

Fig. 5. Complete fabrication process: (a) 1st implanted bare sample with Pt alignment marks, (b) 2nd implantation and anneal, (c) waveguide patterning and etching, (d) Antenna region etching, (e) Gold seed layer deposition, electroplating, and seed layer removal, (f) SU-8 inverse taper overlaid patterning, (g) EO polymer coating and curing.

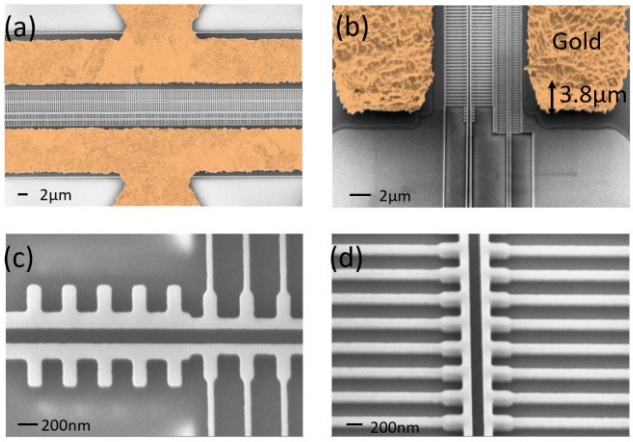

Fig. 6. SEM images of fabricated device: (a Ttop view of MZI structure with antenna (colored with orange), (b) Tilted cross-section view of the MZI with antenna (colored with orange), (c) Top view of 1D SPCW region with 5 sets of step taper, (d) Tilted cross-section view of 1D SPCW.

IV. Device Characterization

A. Transmission spectra measurement and group index calculation

Transmission spectra of the fabricated devices are obtained using a broadband TE-polarized amplified spontaneous emission (ASE) source with 3 dB bandwidth of 1530 nm to 1610 nm and optical spectrum analyzer (OSA). Two lensed fibers are used for light coupling and positioned on motorized 6-axis stage with precise position control by Newport XPS-Q8 motion controller. A testing 300 μm long 1D SPCW coated with EO polymer on the same chip is firstly tested for optical transmission spectrum. Figure 7 shows the normalized transmission spectrum of the EO polymer infiltrated 1D SPCW. A clear band gap at 1569 nm with more than 20 dB extinction ratio can be observed. The lowest optical loss had been measured is 4.39 dB at 1578.32 nm. The ripples showed in the transmission spectrum comes from mode and group index mismatching at the interfaces between slot waveguide and step taper, as well as the step taper and 1D SPCW.

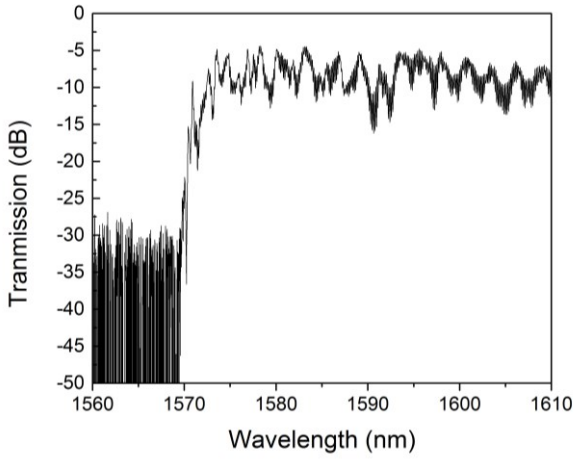

Fig. 7. Measured transmission spectrum of 300 μm long EO polymer infiltrated 1D SPCW.

The transmission spectrum of the poled MZI structure without applying voltage on the electrodes was then measured as shown in Figure 8. Due to the group velocity difference between the two arms and the corresponding optical path difference, interference pattern is observed and plotted in Figure 8. As the group velocity of the 1D SPCW increases at the bandgap, the period of the interference pattern become smaller. The group index of each arm has the relationship [19]:

$$n_{g,PCW} = n_{g,ref} + \frac{\lambda_{min} \times \lambda_{max}}{2 \times L(\lambda_{min} - \lambda_{max})} \quad (1)$$

where the $n_{g,pcw}$ is the group index of the arm with 1D SPCW, and $n_{g,ref} = 3.9$ is the group index of another arm of silicon strip waveguide with teeth. L=300 μm which is the physical length of the phase shifter. The λ_{max} and λ_{min} are the wavelength at local power maxima and minima on the spectrum. As shown in Figure 8, the group index of the 1D SPCW can achieve 19.3 at 1545.75 nm. The optical bandwidth of the slow light region (n_g>10) covers 5.13 nm, from 1545.75 nm to 1550.853 nm. The measured slow light wavelength region is blue-shifted 18 nm compared to simulation due to fabrication errors.

This article has been accepted for publication in a future issue of this journal, but has not been fully edited. Content may change prior to final publication. Citation information: DOI 10.1109/JLT.2017.2784382, Journal of Lightwave Technology

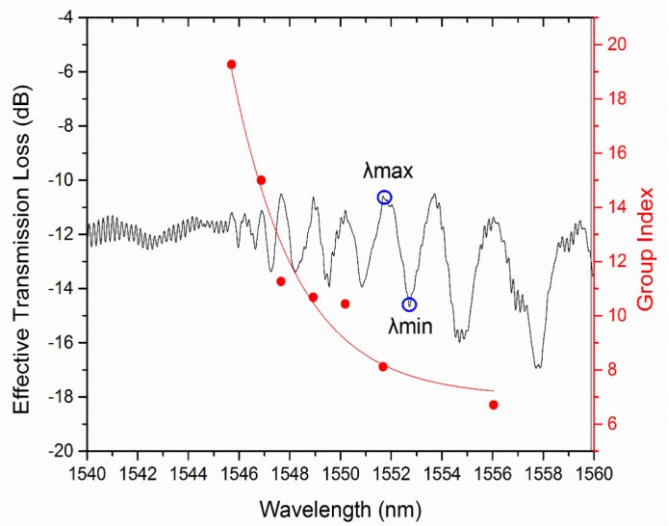

Fig. 8. Measured transmission spectrum of EO polymer infiltrated MZI structure and the calculated group indices of the 1D SPCW as a function of wavelength.

B. Antenna frequency response measurement

The bowtie antenna is characterized using HP-8510C vector network analyzer (VNA) and GS high speed probe for S_{11} parameter to understand the frequency response of the bowtie antenna. As shown in Figure 9, the measured S_{11} parameter shows good accordance with simulation results which were performed using ANSYS HFSS with detailed setting reported in other papers [25-29].A dip at 14.086 GHz with 3 dB RF bandwidth of 4.84 GHz. The electrical bandwidth of the sensor device is primarily determined by the bowtie antenna since other factors such as EO polymer frequency response and RC delay of the doped silicon won't limit the sensor bandwidth. Therefore, bowtie antenna frequency response can be treated as the sensor frequency response.

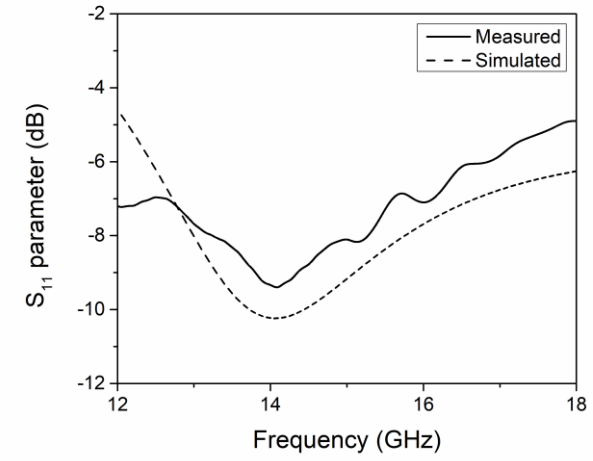

Fig. 9. Measured and simulated S11 parameter from in K_u band.

C. EM wave sensing measurements

The EM wave sensing experiment is then conducted and the setup is shown in Figure 10. Same VNA is used as a microwave source. The microwave signal is amplified and then fed into a standard gain horn antenna. The horn antenna emits wireless microwave signal at normal incidence with respect to the surface of the sensor. The distance of the horn antenna and the device is greater than 40 cm to ensure the far field radiation distance calculated by $2D^2/\lambda$, where D is the largest dimension of the horn antenna aperture and λ is the wavelength of the microwave signal. A polarized tunable laser source at center wavelength of 1546nm is fed into the device using the same setup as the passive optical spectrum testing. The output light of the device is connected to New Focus 1014 high speed photo diode (PD) and then connected to HP 8563E microwave spectrum analyzer (MSA) to analyze the signal. As shown in Figure 11, when 6.7 dBm 14.1 GHz signal inputs into the antenna, the MSA reads -82.8 dBm which indicates the optical signal is successfully modulated at the same frequency.

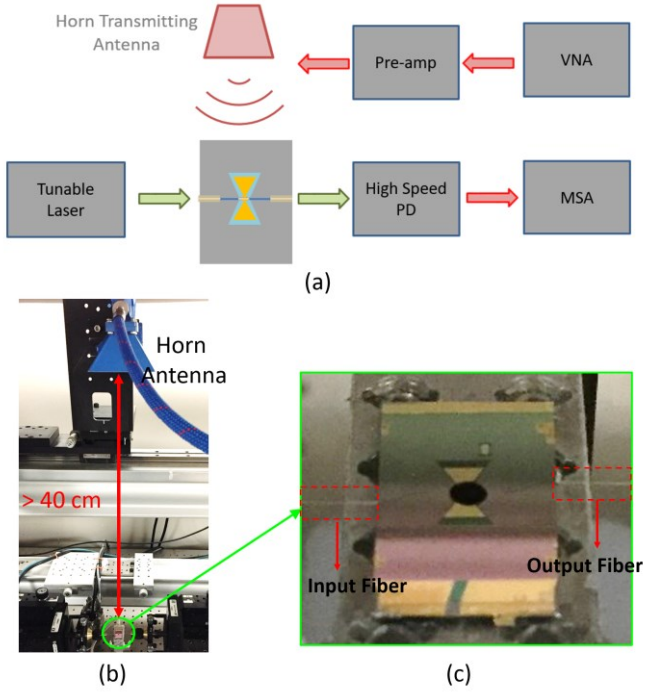

Fig. 10. (a) Schematic of EM wave sensing testing setup. Green path: optical signal; Red path: electrical signal. (b) Horn antenna as transmitting antenna at far field distance with respect to the device. (c) The zoom in image of the device and two coupling lensed fiber.

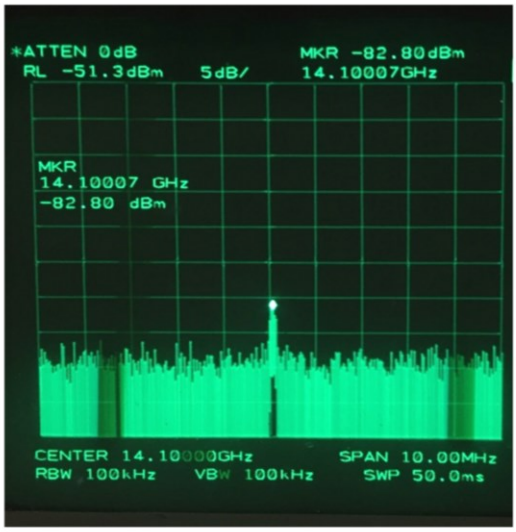

Fig. 11. MSA reading at 14.1GHz from high speed PD when the input signal of the horn antenna is 6.7dBm.

This article has been accepted for publication in a future issue of this journal, but has not been fully edited. Content may change prior to final publication. Citation information: DOI 10.1109/JLT.2017.2784382, Journal of Lightwave Technology

A normalized factor is considered to exclude to frequency response caused by horn antenna and obtain the real response of the sensor. Normalized factors (NF) at K_u band are derived from the equation[30]:

$$\mathrm{NF} = \frac{P}{P_{max}} = (1 - |\Gamma|^2)G \quad (2)$$

where the NF is the power at the interested frequency divided by the power maxima within the frequency range. Γ is the reflection coefficient at the horn antenna port, and G is the antenna gain. The Γ values are obtained using measured S_{11} value with cable and antenna. G is simulated antenna gain in the normal incident direction. In order to determine the limit of detection of the EM wave sensor in terms of electromagnetic wave power density, the relationship between the power density at certain distance away from the horn antenna and the input microwave power into horn antenna can be firstly derived [31]:

$$\mathrm{S} = \frac{G \times P}{4\pi R^2} \quad (3)$$

where S is the averaged power density (Poynting vector) in the unit of mW/m^2, G=10 dB is the horn antenna realized gain with NF at the nominal direction, P is the microwave power input into the horn antenna, and R=42 cm is the distance between horn antenna phase center and sample. Limit of detection of the sensor can be measured by decreasing the input microwave power into the horn antenna when the MSA reading reaches the noise floor. As shown in Figure 12, the sensing signal from the reading of MSA versus the input microwave power into the horn antenna is plotted with error bars which are mainly caused by end-fire coupling stages and high speed photodiode. When the input microwave power decrease to 4.31 mW/m^2, the MSA reading is -87.43 dBm which is less than 1 dB higher than noise floor. Therefore, limit of detection of the device at 14.1 GHz is 4.31 mW/m^2, which is corresponding to the minimum detectable electric field of 1.8 V/m using the equation [32]:

$$|E| = \sqrt{\frac{2S}{\varepsilon_0 \varepsilon_r C}} \quad (4)$$

where ε_0 is vacuum dielectric constant, ε_r is the dielectric constant of air, c is the speed of light, and S is the averaged power density from the horn antenna. The power of the RF tone from the RF spectrum analyzer is weak, because the on-chip bowtie antenna only captures a small portion of the RF power emitted from the horn antenna.

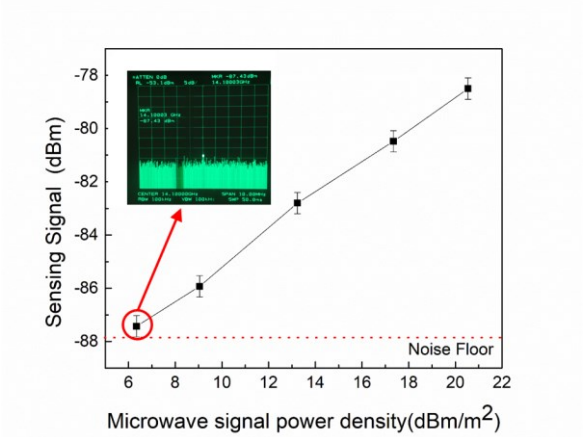

Fig. 12. Measured sensing signal reading from MSA versus different microwave input signal power with error bars.

V. Conclusion

We proposed and experimentally demonstrated a compact and sensitive on-chip EM wave photonic sensor operating at 14.1 GHz with 4.84 GHz RF bandwidth. The sensor is based on bowtie antenna coupled MZI structure with one arm of low loss and slow-light enhanced EO polymer infiltrated 1D SPCW and the other arm of silicon strip waveguide with teeth. The silicon teeth design in both arms are for electrical connection purpose with careful implantation design so that voltage drop can occur in 150 nm slot region. The sensor device has advantages of compact size (4.6 mm × 4.8 mm), low optical loss (~10 dB), and high sensitivity; therefore, has potential to be adopted in various communication and sensing applications. The limit of detection at 14.1 GHz is 4.31 mW/m^2, which is corresponding to minimum detectable electric field of 1.8 V/m.

References

[1] C.-Y. Lin, A. X. Wang, B. S. Lee, X. Zhang, and R. T. Chen, "High dynamic range electric field sensor for electromagnetic pulse detection," *Optics Express,* vol. 19, pp. 17372-17377, 2011/08/29 2011.

[2] O. D. Herrera, K.-J. Kim, R. Voorakaranam, R. Himmelhuber, S. Wang, V. Demir*, et al.*, "Silica/electro-optic polymer optical modulator with integrated antenna for microwave receiving," *Journal of Lightwave Technology,* vol. 32, pp. 3861-3867, 2014.

[3] Z. Xingyu, A. Hosseini, H. Subbaraman, W. Shiyi, Z. Qiwen, L. Jingdong*, et al.*, "Integrated Photonic Electromagnetic Field Sensor Based on Broadband Bowtie Antenna Coupled Silicon Organic Hybrid Modulator," *Lightwave Technology, Journal of,* vol. 32, pp. 3774-3784, 2014.

[4] Y. Salamin, W. Heni, C. Haffner, Y. Fedoryshyn, C. Hoessbacher, R. Bonjour*, et al.*, "Direct Conversion of Free Space Millimeter Waves to Optical Domain by Plasmonic Modulator Antenna," *Nano Letters,* vol. 15, pp. 8342-8346, 2015/12/09 2015.

[5] G. Gustafsson, R. Boström, B. Holback, G. Holmgren, A. Lundgren, K. Stasiewicz*, et al.*, "The Electric Field and Wave Experiment for the Cluster Mission," in *The*

Cluster and Phoenix Missions, C. P. Escoubet, C. T. Russell, and R. Schmidt, Eds., ed Dordrecht: Springer Netherlands, 1997, pp. 137-156.

[6] H. Liu, J. Yu, P. Huggard, and B. Alderman, "A Multichannel THz Detector Using Integrated Bow-Tie Antennas," *International Journal of Antennas and Propagation,* vol. 2013, p. 8, 2013.

[7] V. M. N. Passaro, F. Dell'Olio, and F. De Leonardis, "Electromagnetic field photonic sensors," *Progress in Quantum Electronics,* vol. 30, pp. 45-73, // 2006.

[8] H. Murata, R. Miyanaka, and Y. Okamura, "Wireless space-division-multiplexed signal discrimination device using electro-optic modulator with antenna-coupled electrodes and polarization-reversed structures," *International Journal of Microwave and Wireless Technologies,* vol. 4, pp. 399-405, 2012.

[9] A. J. Seeds, H. Shams, M. J. Fice, and C. C. Renaud, "Terahertz photonics for wireless communications," *Journal of Lightwave Technology,* vol. 33, pp. 579-587, 2015.

[10] V. S. Ilchenko, A. A. Savchenkov, A. B. Matsko, and L. Maleki, "Whispering-gallery-mode electro-optic modulator and photonic microwave receiver," *Journal of the Optical Society of America B,* vol. 20, pp. 333-342, 2003/02/01 2003.

[11] X. Zhang, C.-J. Chung, A. Hosseini, H. Subbaraman, J. Luo, A. K. Jen*, et al.*, "High performance optical modulator based on electro-optic polymer filled silicon slot photonic crystal waveguide," *Journal of Lightwave Technology,* vol. 34, pp. 2941-2951, 2016.

[12] S. Koeber, R. Palmer, M. Lauermann, W. Heni, D. L. Elder, D. Korn*, et al.*, "Femtojoule electro-optic modulation using a silicon-organic hybrid device," *Light Sci Appl,* vol. 4, p. e255, 02/27/online 2015.

[13] J. Tian, S. Yu, W. Yan, and M. Qiu, "Broadband high-efficiency surface-plasmon-polariton coupler with silicon-metal interface," *Applied Physics Letters,* vol. 95, p. 013504, 2009.

[14] EnamiY, C. T. Derose, MathineD, LoychikC, GreenleeC, R. A. Norwood*, et al.*, "Hybrid polymer//sol-gel waveguide modulators with exceptionally large electro-optic coefficients," *Nat Photon,* vol. 1, pp. 180-185, 03//print 2007.

[15] X. Zhang, A. Hosseini, S. Chakravarty, J. Luo, A. K. Y. Jen, and R. T. Chen, "Wide optical spectrum range, subvolt, compact modulator based on an electro-optic polymer refilled silicon slot photonic crystal waveguide," *Optics Letters,* vol. 38, pp. 4931-4934, 2013/11/15 2013.

[16] C.-Y. Lin, A. X. Wang, W.-C. Lai, J. L. Covey, S. Chakravarty, and R. T. Chen, "Coupling loss minimization of slow light slotted photonic crystal waveguides using mode matching with continuous group index perturbation," *Optics Letters,* vol. 37, pp. 232-234, 2012/01/15 2012.

[17] A. D. Falco, M. Massari, M. G. Scullion, S. A. Schulz, F. Romanato, and T. F. Krauss, "Propagation Losses of Slotted Photonic Crystal Waveguides," *IEEE Photonics Journal,* vol. 4, pp. 1536-1541, 2012.

[18] S.-i. Inoue and A. Otomo, "Electro-optic polymer/silicon hybrid slow light modulator based on one-dimensional photonic crystal waveguides," *Applied Physics Letters,* vol. 103, p. 171101, 2013.

[19] H. Yan, X. Xu, C.-J. Chung, H. Subbaraman, Z. Pan, S. Chakravarty*, et al.*, "One-dimensional photonic crystal slot waveguide for silicon-organic hybrid electro-optic modulators," *Optics Letters,* vol. 41, pp. 5466-5469, 2016/12/01 2016.

[20] A. D. Panagopoulos, P.-D. M. Arapoglou, and P. G. Cottis, "Satellite communications at Ku, Ka, and V bands: Propagation impairments and mitigation techniques," *IEEE Communications Surveys & Tutorials,* vol. 6, 2004.

[21] C.-J. Chung, H. Subbaraman, X. Zhang, H. Yan, J. Luo, A. K. Y. Jen*, et al.*, "Towards a fully packaged high-performance RF sensor featuring slotted photonic crystal waveguides," 2016, pp. 97471V-97471V-12.

[22] X. Zhang, C. J. Chung, S. Wang, H. Subbaraman, Z. Pan, Q. Zhan*, et al.*, "Integrated Broadband Bowtie Antenna on Transparent Silica Substrate," *IEEE Antennas and Wireless Propagation Letters,* vol. 15, pp. 1377-1381, 2016.

[23] S. Wang and Q. Zhan, "Modified bow-tie antenna with strong broadband field enhancement for RF photonic applications," 2013, pp. 88061V-88061V-6.

[24] J. K. Doylend, P. E. Jessop, and A. P. Knights, "Optical attenuation in ion-implanted silicon waveguide racetrack resonators," *Optics Express,* vol. 19, pp. 14913-14918, 2011/08/01 2011.

[25] D. Gao and Z. Zhou, "Nonlinear equation method for band structure calculations of photonic crystal slabs," *Applied Physics Letters,* vol. 88, p. 163105, 2006.

[26] W. Perrins, D. McKenzie, and R. McPhedran, "Transport properties of regular arrays of cylinders," in *Proceedings of the Royal Society of London A: Mathematical, Physical and Engineering Sciences*, 1979, pp. 207-225.

[27] X. Zhang, S. Wang, H. Subbaraman, Q. Zhan, Z. Pan, C.-j. Chung*, et al.*, "Integrated broadband bowtie antenna on transparent substrate," *arXiv preprint arXiv:1503.01907,* 2015.

[28] X. Zhang, "Silicon-polymer hybrid integrated microwave photonic devices for optical interconnects and electromagnetic wave detection," 2015.

[29] X. Wang, C.-Y. Lin, S. Chakravarty, J. Luo, A. K. Y. Jen, and R. T. Chen, "Effective in-device r33 of 735 pm/V on electro-optic polymer infiltrated silicon photonic crystal slot waveguides," *Optics Letters,* vol. 36, pp. 882-884, 2011/03/15 2011.

[30] C. A. Balanis, *Antenna theory: analysis and design*: John Wiley & Sons, 2016.

[31] D. M. Pozar, *Microwave Engineering*: Wiley, 2012.

[32] A. Chen and E. Murphy, *Broadband optical modulators: science, technology, and applications*: CRC press, 2011.

Chi-Jui Chung received the B.S. degree in mechanical engineering from National Chiao Tung University, Hsinchu, Taiwan, in 2009 and the M.S. degree in power mechanical

engineering from National Tsing Hua University, Hsinchu, Taiwan, in 2011. From 2011 to 2014, he was with the Electronics and Opto-Electronics Research Laboratories, Industrial Technology Research Institute, Hsinchu, Taiwan. He is currently working toward the Ph.D. degree at the University of Texas at Austin, TX, USA. His current research interests include sub-volt photonic crystal waveguide modulators, broadband electromagnetic field sensors, and silicon based photonic true time delay system.

Xiaochuan Xu (M'15) received the B.S. and M.S. degrees in electrical engineering from the Harbin Institute of Technology, Harbin, China, in 2006 and 2009, respectively, and the Ph.D. degree in electrical and computer engineering from the University of Texas, Austin, TX, USA, in 2013. His current research interests include flexible photonics, nonlinear optics, fiber optics, and silicon photonics. Dr. Xu has published over 90 peer-reviewed journal and conference papers, and holds three US patents. He is a member of IEEE, OSA and SPIE.

Zeyu Pan (S'12) received the B.S. degree in optical information science and technology from the Nanjing University of Science and Technology, Nanjing, China, in 2010, and the M.S. degree in electrical and computer engineering from the University of Alabama in Huntsville, Huntsville, AL, USA, in 2013. He is currently working toward the Ph.D. degree in the University of Texas at Austin, Austin, TX, USA. He has authored and coauthored about 38 journal and conference publications. His interests include the polymer waveguide, printed flexible electronics and photonics, patch array antennas, thermo- and electrooptic polymers, phase delay, nanofabrication, RF measurements, inkjet printing, imprinting, and numerical algorithm

Farzad Mokhtari-Koushyar obtained the M.Sc. degree from Department of Electronics and Communication Engineering, Sharif University of Technology, Tehran, Iran. He is now pursing the PhD degree in Department of Electrical and Computer Engineering, University of Texas at Austin, Austin, TX, USA. His research interests include antennas, microwave devices and circuits, printed electronics, and microwave photonics.

Rui Wang obtained the B.S. degree from Department of Microelectronics, Peking University and the M.Sc. degree from Department of Electrical and Computer Engineering, McMaster University. He is now pursing the PhD degree in Department of Electrical and Computer Engineering, University of Texas at Austin, Austin, TX, USA.

Hai Yan received his B.S. degree in optical information science and technology from Huazhong University of Science and Technology, Wuhan, China, in 2010 and M.S. degree in electronic engineering from Tsinghua University, Beijing, China, in 2013. He is currently working towards his Ph.D. degree at the University of Texas at Austin, TX, USA. His research interests include silicon photonics, nonlinear optics, integrated photonic biosensors, silicon-organic hybrid nanophotonic devices.

Harish Subbaraman (M'09) received the M.S. and Ph.D. degrees in electrical engineering from the University of Texas, Austin, TX, USA, in 2006 and 2009, respectively. With a strong background in RF photonics and Xband Phased Array Antennas, he has been working on optical true-time-delay feed networks for phased array antennas for the past 8 years. Throughout these years, he has laid a solid foundation in both theory and experimental skills. His current research interests include printing and silicon nanomembrane-based flexible electronic and photonic devices, polymer photonics, slow-light photonic crystal waveguides, carbon nanotube, and silicon nanoparticle nanofilm-based ink-jet printed flexible electronics, and RF photonics. He has served as a PI on 10 SBIR/STTR Phase I/II projects from NASA, Air Force, and Navy. He has more than 85 publications in refereed journals and conferences

Ray T. Chen (M'91–SM'98–F'04) Ray Chen is the Keys and Joan Curry/Cullen Trust Endowed Chair at The University of Texas Austin. He is the director of the Nanophotonics and Optical Interconnects Research Lab, at the Microelectronics Research Center. He is also the director of the AFOSR MURI-Center for Silicon Nanomembrane involving faculty from Stanford, UIUC, Rutgers, and UT Austin. He received his BS degree in Physics in 1980 from the National Tsing Hua University in Taiwan, his MS degree in physics in 1983, and his PhD degree in Electrical Engineering in 1988, both from the University of California. He joined UT Austin in 1992 to start the optical interconnect research program. From 1988 to 1992 Chen worked as a research scientist, manager, and director of the Department of Electro-Optic Engineering at the Physical Optics Corporation in Torrance, California.

Chen served as the CTO, Founder, and Chairman of the Board of Radiant Research, Inc. from 2000 to 2001, where he raised 18 million dollars A-Round funding to commercialize polymer-based photonic devices involving over twenty patents, which were acquired by Finisar in 2002, a publicly traded company in the Silicon Valley (NASDAQ:FNSR). He also serves as the founder and Chairman of the Board of Omega Optics Inc. since its initiation in 2001. Omega Optics has received over five million dollars in research funding. His research work has been awarded over 135 research grants and contracts from such sponsors as Army, Navy, Air Force, DARPA, MDA, NSA, NSF, DOE, EPA, NIST, NIH, NASA, the State of Texas, and private industry. The research topics are focused on four main subjects: (1) Nano-photonic passive and active devices for bio- and EM-wave sensing and interconnect applications, (2) Thin film guided-wave optical interconnection and packaging for 2D and 3D laser beam routing and steering, (3) True time delay (TTD) wide band phased array antenna (PAA), and (4). 3D printed micro-electronics and photonics. Experiences garnered through these programs are pivotal elements for his research and further commercialization.

Chen's group at UT Austin has reported its research findings in more than 860 published papers, including over 100 invited papers. He holds over 35 patents. He has chaired or been a program-committee member for more than 110 domestic and international conferences organized by IEEE, SPIE (The International Society of Optical Engineering), OSA, and PSC.

He has served as an editor, co-editor or coauthor for over twenty books. Chen has also served as a consultant for various federal agencies and private companies and delivered numerous invited talks to professional societies. Chen is a Fellow of IEEE, OSA, and SPIE. He was the recipient of the 1987 UC Regent's Dissertation Fellowship and the 1999 UT Engineering Foundation Faculty Award, for his contributions in research, teaching and services. He received the honorary citizenship award in 2003 from the Austin city council for his contribution in community service. He was also the recipient of the 2008 IEEE Teaching Award, and the 2010 IEEE HKN Loudest Professor Award. 2013 NASA Certified Technical Achievement Award for contribution on moon surveillance conformable phased array antenna. During his undergraduate years at the National Tsing Hua University he led the 1979 university debate team to the Championship of the Taiwan College-Cup Debate Contest.

Chen has supervised and graduated 48 PhD students from his research group at UT Austin. Many of them are currently professors in the major research universities in USA and abroad.